



## Article

# Analysis of the Flow Capacity of Variable Cycle Split Fans at the Middle Speed

Guangfeng An <sup>1,2,3</sup> , Rui Zhou <sup>1</sup>, Xianjun Yu <sup>1,2,3,\*</sup> , Baojie Liu <sup>1,2,3</sup> and Guanghan Wu <sup>1,4</sup>

<sup>1</sup> Research Institute of Aero-Engine, Beihang University, Beijing 102206, China; guangfeng@buaa.edu.cn (G.A.); zhourui2032133@buaa.edu.cn (R.Z.); liubj@buaa.edu.cn (B.L.); 15652591152@163.com (G.W.)

<sup>2</sup> National Key Laboratory of Science and Technology on Aero-Engine Aero-Thermodynamics, Beihang University, Beijing 102206, China

<sup>3</sup> Frontiers Science Center for Super-Cycle Aeroengine's Aerothermodynamics, Beihang University, Beijing 102206, China

<sup>4</sup> Shenyang Engine Research Institute, Aero Engine Corporation of China, Shenyang 110015, China

\* Correspondence: yuxj@buaa.edu.cn

**Abstract:** The next-generation variable cycle engine imposes stricter requirements on a fan's flow capacity at the middle speed. To tackle this challenge, the implementation of split fans presents as a potential solution. In the present study, we conducted numerical simulations using the commercial software NUMECA to investigate the aerodynamic performance variation with bypass ratios for variable cycle split fans in "1 + 2" and "2 + 1" configurations at 80% rpm. The results indicate that the flow capacity of the split fans exhibits an increasing trend with a rise in the bypass ratio at 80% rpm and subsequently stabilizes upon reaching a certain bypass ratio. Specifically, the flow capacity of the "2 + 1" split fans is particularly stronger at the small bypass ratios, whereas the "1 + 2" split fans exhibit superior maximum flow capacity at the high bypass ratios. Additionally, there is a significantly faster increase in the flow capacity of the "1 + 2" split fans compared to that of the "2 + 1" split fans. Furthermore, when the flow capacity of the split fans reaches its maximum, both the efficiency and stall margin achieve their optimal values, indicating that the corresponding bypass ratio is optimal.



**Citation:** An, G.; Zhou, R.; Yu, X.; Liu, B.; Wu, G. Analysis of the Flow Capacity of Variable Cycle Split Fans at the Middle Speed. *Energies* **2024**, *17*, 1194. <https://doi.org/10.3390/en17051194>

Academic Editors: Michele Marconcini and Roberto Pacciani

Received: 4 January 2024

Revised: 10 February 2024

Accepted: 23 February 2024

Published: 2 March 2024



**Copyright:** © 2024 by the authors. Licensee MDPI, Basel, Switzerland. This article is an open access article distributed under the terms and conditions of the Creative Commons Attribution (CC BY) license (<https://creativecommons.org/licenses/by/4.0/>).

**Keywords:** variable cycle split fans; compressor configuration; maximum flow capacity; optimal bypass ratio

## 1. Introduction

The three-stream variable cycle engine offers a higher bypass ratio, increased flow capacity, reduced overflow resistance, wider operating range, lower fuel consumption rate, and more pronounced economic improvement between its maximum state and subsonic cruise state [1–4]. Research findings indicate that variable cycle split fans exhibit enhanced flow capability at low speeds, thereby significantly augmenting the variable cycle capability of a three-stream variable cycle engine when employed as its fan configuration [5–7].

A variable cycle split fan divides a low-pressure fan into front and rear parts. A third bypass with a regulating valve is added at the outlet of the front fan, allowing for control of the bypass ratio by adjusting the mass flow in the inner ducts and the third bypass [8]. The distribution effect of the bypass is crucial in achieving enhanced flow capability of variable cycle split fans at low speeds. Therefore, it is imperative to investigate the regulation patterns and typical aerodynamic characteristics of the split fans at low speeds. However, current research primarily focuses on considering variable cycle split fans as components within comprehensive modeling and control studies of three-stream variable cycle engines [9,10], lacking investigations into how changes in the bypass ratio influence the flow capability of split fans at low speeds.

Similar to the aerodynamic configuration of the variable cycle split fan, the core engine-driven fan (CDFS) is located before the high-pressure compressor (HPC) and shares the same high-pressure shaft [11]. Additionally, a bypass is added at the outlet to achieve variable cycle capability through bypass ratio adjustment [12]. Therefore, studying the impact of bypass ratio adjustment on the aerodynamic performance of a CDFS and drawing relevant conclusions can provide valuable insights for exploring the flow capacity of split fans at low speeds with varying bypass ratios. Through three-dimensional numerical simulation and analysis of the throttling characteristics of the inner and outer ducts of a CDFS at design speed, it can be demonstrated that bypass flow throttling can realize a large range of bypass ratio adjustment, while primary flow throttling can realize a large range of total pressure ratio adjustment. A secondary bypass outlet guide vane (OGV)'s stall and CDFS' chock are the limiting factors of bypass ratio adjustment, and an HPC's stall and chock limit total pressure ratio adjustment [13]. Due to the characteristics of CDFS and HPC with a single shaft and double ducts, there exists a significant performance interaction between the CDFS and the HPC. When the bypass ratio increases, the flow rate of the CDFS exhibits an increase, leading to an overall enhancement in the total efficiency of both the CDFS and HPC. Simultaneously, there is a decrease in the matching pressure ratio at the operating point of the CDFS, while an increase is observed in the matching pressure ratio at the operating point of the HPC. Conversely, when the bypass ratio decreases, these performance parameters exhibit opposite trends [14]. Moreover, the alteration in the bypass ratio will influence the uniformity of span-wise flow at the outlet of the CDFS, consequently leading to a change in span-wise matching at the inlet stage of the HPC; however, it exerts a negligible impact on the span-wise matching state of the CDFS [15].

It should be noted that although the aerodynamic configuration of split fans and a CDFS may appear similar, they differ fundamentally in several aspects. Firstly, the downstream section of the CDFS comprises a multi-stage HPC, whereas the rear fan of the split fan typically only has one or two stages, resulting in significantly fewer multi-stage effects compared to the HPC. Secondly, the CDFS operates at lower loads than conventional fans, making it challenging to maintain efficiency during various operating conditions. On the other hand, split fans operate with a load coefficient closer to that of a conventional fan and require higher flow rates at low speeds. Additionally, there are differences in how their bypass ratios vary under different operating conditions. Therefore, research conclusions regarding a CDFS cannot be directly applied to explain flow issues related to split fans. Henceforth, this study aims to investigate how variable cycle split influences flow capacity and internal flow mechanisms under medium–low speeds.

Consequently, the specific research objects of this paper are “1 + 2” and “2 + 1” split fans. Numerical simulations were conducted to analyze the variation in maximum flow capacity, efficiency, and stall margin of split fans with bypass ratios at 80% rpm. These findings will provide essential technical support for the practical implementation of variable cycle split fans in the next-generation variable cycle engine.

## 2. Research Object and Numerical Method

The 100% RPM characteristics of two distinct configurations of split fans are presented in this section, along with the methodology for adjusting the aspect ratio at 80% RPM. To ensure we obtained comprehensive aerodynamic characteristics and detailed flow field information, a numerical simulation was conducted using the commercial software NUMECA 9.0-2 in this study. Additionally, the experimental verification results of the numerical method and research findings on grid independence are provided to enhance the reliability of the numerical results.

### 2.1. Research Object

As illustrated in Figure 1, “2 + 1” split fans consists of two-stage front fans and a one-stage rear fan, while the “1 + 2” split fans comprise a one-stage front fan and two-stage rear fans, where  $R_i$  refers to the rotor blade row and  $S_i$  refers to the stator blade row. The

front and rear fans operate at an identical physical speed. This paper investigates the regulation of the bypass ratio for split fans at 80% rpm. The inlet guide vane (IGV) and stators remained fixed, and the adjustment of the split fan's bypass ratio was achieved solely by modifying the back pressure of the inner duct and bypass. In order to ensure the comparability of the research results, the bypass ratio at the design point and the flow and pressure ratio at all stages of the two split fans studied and compared in this paper were the same, and the difference in the efficiency was only 0.8%. Additionally, the design parameters of the split fans with different configurations are presented in Table 1, which fall within a reasonable range. The total pressure ratio of split fans is defined as the ratio of the exit total pressure of the inner duct to the inlet total pressure of the front fan. Meanwhile, the aerodynamic parameters at the front fans' inlet and the inner duct's outlet were utilized for calculating the efficiency.

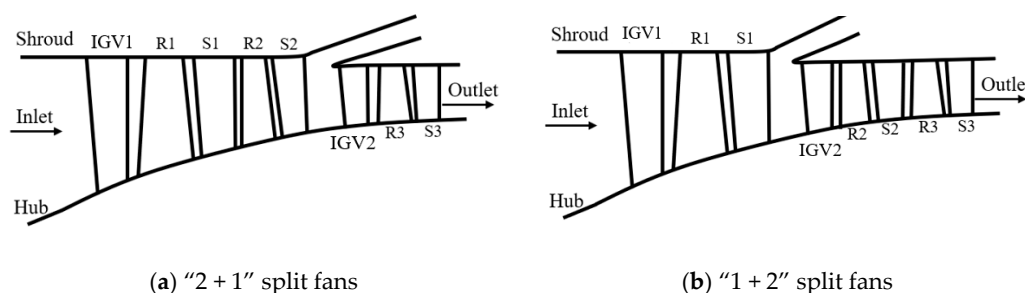


Figure 1. Meridian diagrams of the variable cycle split fans.

Table 1. Design parameters for different split fans.

	"2 + 1" Split Fans			"1 + 2" Split Fans		
	Stage 1	Stage 2	Stage 3	Stage 1	Stage 2	Stage 3
Loading coefficient, $\psi$ (-)	0.245	0.270	0.257	0.245	0.283	0.261
Flow coefficient, $\varphi$ (-)	0.624	0.529	0.536	0.624	0.534	0.506
Degree of reaction, DR (-)	0.828	0.827	0.740	0.830	0.856	0.760
Tangential velocity—tip (m/s)	508	482	456	508	474	456
Hub-to-tip ratio (-)	0.37	0.61	0.76	0.37	0.64	0.74
Bypass ratio (-)		0.13			0.13	

## 2.2. Numerical Method

In this study, the commercial software NUMECA 9.0-2 was utilized for conducting three-dimensional numerical calculations of the fans. A numerical grid was generated using AutoGrid 5, as shown in Figure 2, with the adoption of O4H topology in the blade passage, butterfly topology at the blade tip gap, and C-type topology at the splitter. The tip clearance of the rotor was 0.5 mm, while the lengths of both the inlet and outlet domains were double those of their corresponding IGV/stator components' chord lengths. Additionally, to enhance calculation accuracy and capture flow field details more effectively, local encryption of the blade surface, wheel hub, and casing wall was implemented through the appropriate settings. Ultimately, the grid was clustered at the near-wall region to satisfy the requirements of the turbulent model, as the  $y^+$  of the first grid off-wall was below 5.

The FINE/TURBO 9.0 module was employed to conduct steady numerical research on the split fan model. The numerical method utilized was the steady Reynolds-averaged Navier-Stokes (RANS) time-averaged equations, coupled with the Spalart-Allmaras (S-A) turbulence model. Additionally, multi-grid technology was utilized to improve convergence. The S-A turbulence model was selected for the numerical calculation of the split fans because it has been proven that the flow rate, pressure ratio, and efficiency in the

numerical calculation of Rotor 67 (R67) are close to its experimental results [16], as shown in Figure 3. The present paper defines efficiency ( $\eta$ ) as the following:

$$\eta = \frac{(\pi^{k-1/k} - 1)}{\theta - 1} \quad (1)$$

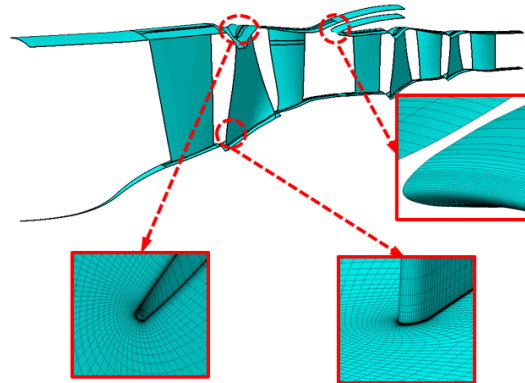


Figure 2. Numerical grids of the “1 + 2” split fans.

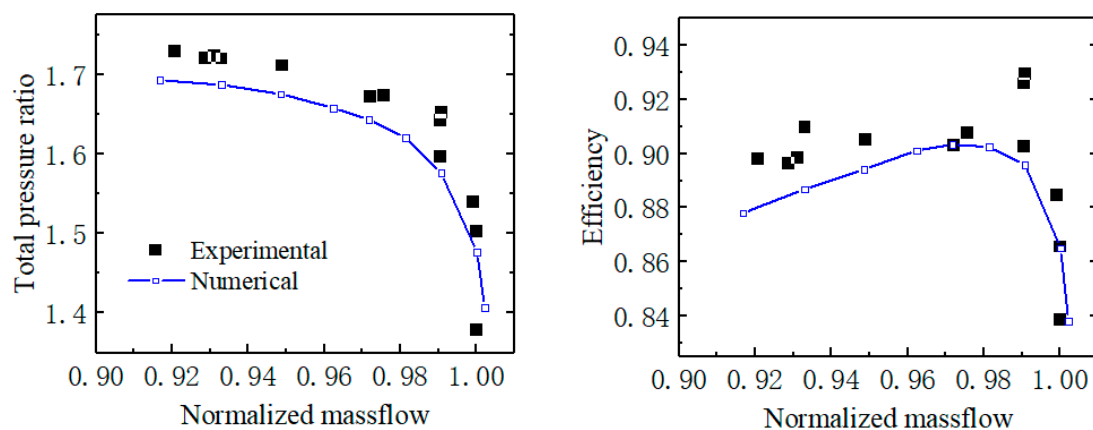
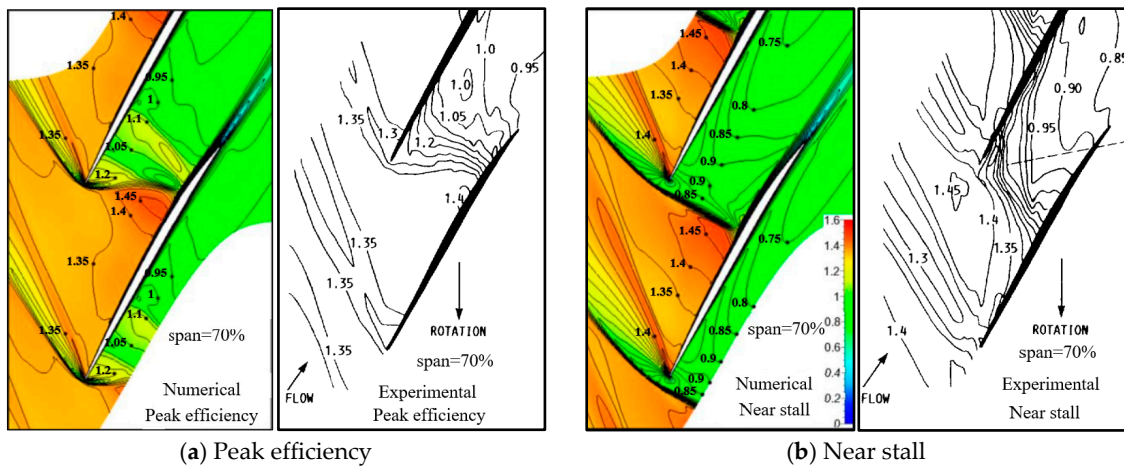


Figure 3. Numerical results and experimental data of Rotor 67 (data are from references [16,17]).

Meanwhile, important flow phenomena at typical operating points of R67 like the leading bow shock and passage shock captured by this numerical method were also close to the experimental results, as shown in Figure 4. Therefore, the numerical method used in this study can ensure the reliability of the numerical results. Additionally, the interface between the rotor and the stator was set as non-reflecting 2D. For the inlet boundary condition, a uniform distribution of air with consistent properties was imposed as inflow in the axial direction, characterized by a total temperature of 288.15 K and a total pressure of 101,325 Pa. Regarding the outlet boundary condition, the radial equilibrium option was employed with specific static pressure specified at the central location.

To determine the appropriate grid resolution, mesh independence studies were performed on two split fans. As shown in Table 2, four different mesh resolutions were studied, with the total number of grids varying from 3 billion to 8 billion. The number of stream-wise, pitch-wise, and pitch-wise nodes across the O-block increased proportionally as the number of grids was expanded in the process. The simulation results, as depicted in Figure 5, encompass both the design condition and the near-stall condition. With an increase in mesh number, the aerodynamic parameters of the split fans exhibit a gradual convergence. The relative difference in aerodynamic parameters between Grid 3 and Grid 4 for both configurations of split fans remains within 1%. Therefore, considering computational accuracy and efficiency, this study will employ Grid 3 for calculations.



**Figure 4.** Mach number contours of numerical results and experimental results of Rotor 67 (figures are from references [16,17]).

**Table 2.** Total number of grids for the grid independence study.

	"2 + 1" Split Fans ( $\times 10^6$ )	"1 + 2" Split Fans ( $\times 10^6$ )
Grid 1	3.79	3.82
Grid 2	5.68	5.51
Grid 3	7.11	7.28
Grid 4	8.31	8.40

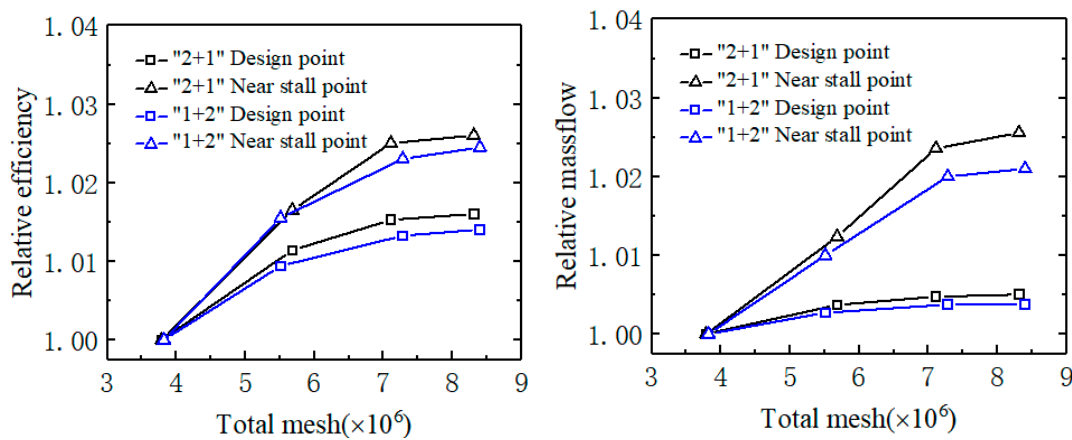


**Figure 5.** Grid independence study of the variable cycle split fans.

### 3. Variation in Aerodynamic Characteristics of the Different Split Fans with Bypass Ratios at the Middle Speed

In this section, the variation in the aerodynamic characteristics of the split fans at 80% rpm was obtained through the numerical simulation, while ensuring a constant bypass ratio, by simultaneously adjusting the back pressure of the inner and outer ducts.

#### 3.1. Variation in Aerodynamic Characteristics of the "2 + 1" Split Fans with Bypass Ratios

The total pressure ratio and efficiency characteristics of the "2 + 1" split fans under different bypass ratios at 80% rpm are depicted in Figure 6. The x-axis represents the ratio of the current corrected flow to the corrected flow at the design point (100% rpm), while the y-axis represents the ratio of the current pressure ratio/efficiency to that at the design point (100% rpm). The airflow capacity and efficiency of split fans with different bypass ratios, represented by Q1, Q2, Q3, and Q4, serve as the crucial operating points for comparative analysis. Figure 7 illustrates characteristics of each stage within the "2 + 1"

split fans operating at 80% rpm. In addition, the bypass ratio defined in this paper refers to the distribution of the mass flow rate in the variable cycle split fans:

$$B = \dot{m}_{bypass} / \dot{m}_{FanII} \tag{2}$$

where the terms  $\dot{m}_{bypass}$  and  $\dot{m}_{FanII}$  represent the respective mass flow rates of the bypass and rear fans.

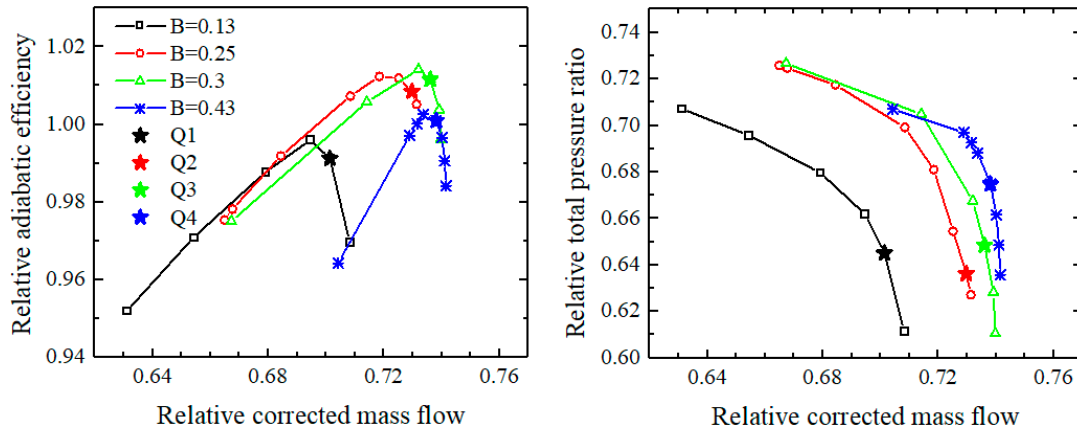


Figure 6. The characteristics of the “2 + 1” split fans at 80% RPM.

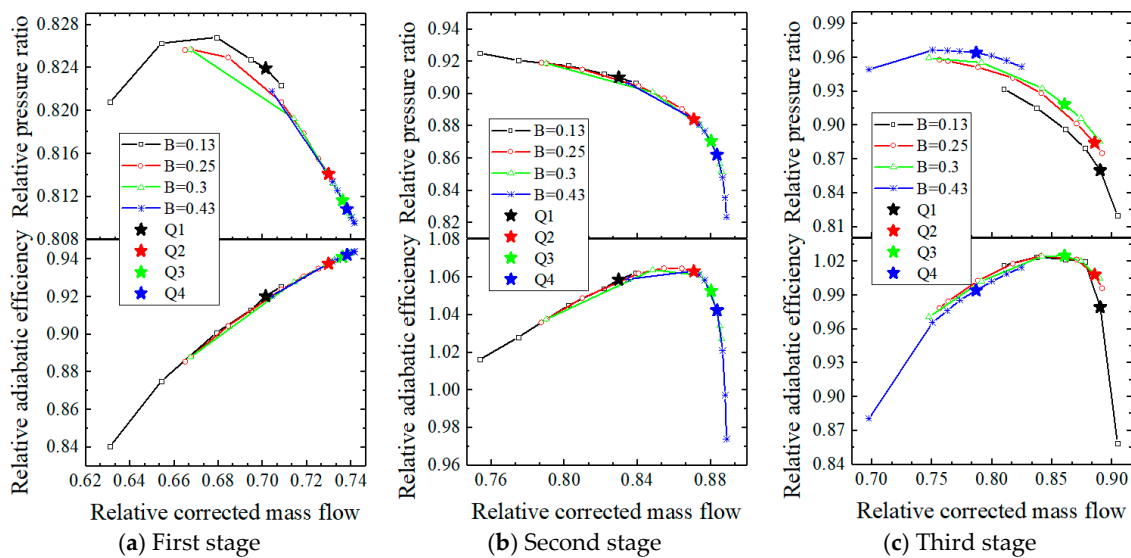


Figure 7. The characteristics for each stage of the “2 + 1” split fans at 80% RPM.

With an increase in the bypass ratio, the overall characteristic lines of the “2 + 1” split fans shift toward the right, resulting in an increased total flow capacity and a peak efficiency that initially rise before declining. At 80% rpm, for small bypass ratios, both the first- and second-stage operating points of the split fans lie to the left of the maximum efficiency point on the characteristic line, approaching near-stall conditions. However, as the bypass ratio increases, these operating points move away from stall boundaries and approach the choking state, as shown in Figure 7a,b (operating points Q1 → Q4). Conversely, when it comes to the small bypass ratios for the third stage of the split fans, their operating point is closer to the choking state. As the bypass ratio increases, the flow at the operating points of the third stage of the split fans decreases and approaches the stall boundaries, as shown in Figure 7c (operating points Q1 → Q4).

### 3.2. Variation in Aerodynamic Characteristics of the “1 + 2” Split Fans with Bypass Ratios

The total pressure ratio and efficiency characteristics of the “1 + 2” split fans under different bypass ratios at 80% rpm are illustrated in Figure 8. P1, P2, P3, and P4 represent the operating points for the comparative analysis of the split fans. Figure 9 presents the characteristics of each stage of the “1 + 2” split fans at 80% rpm.

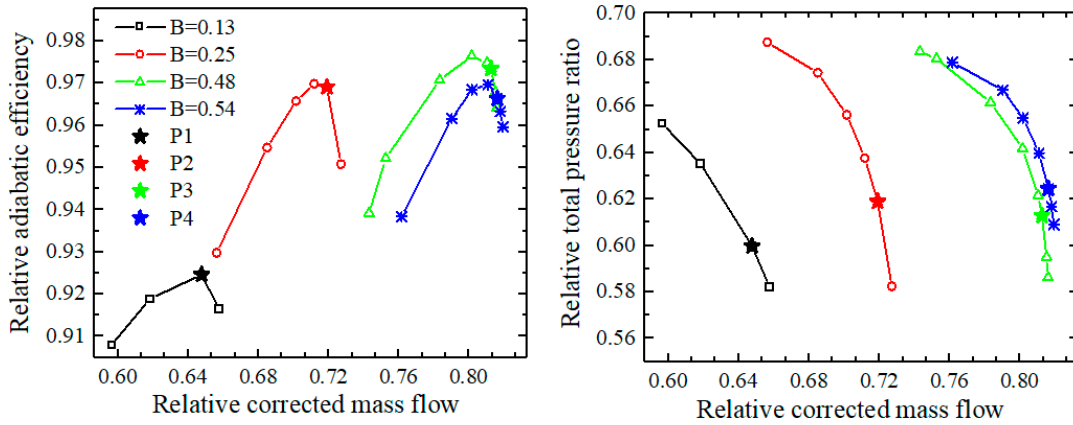


Figure 8. The characteristics of the “1 + 2” split fans at 80% RPM.

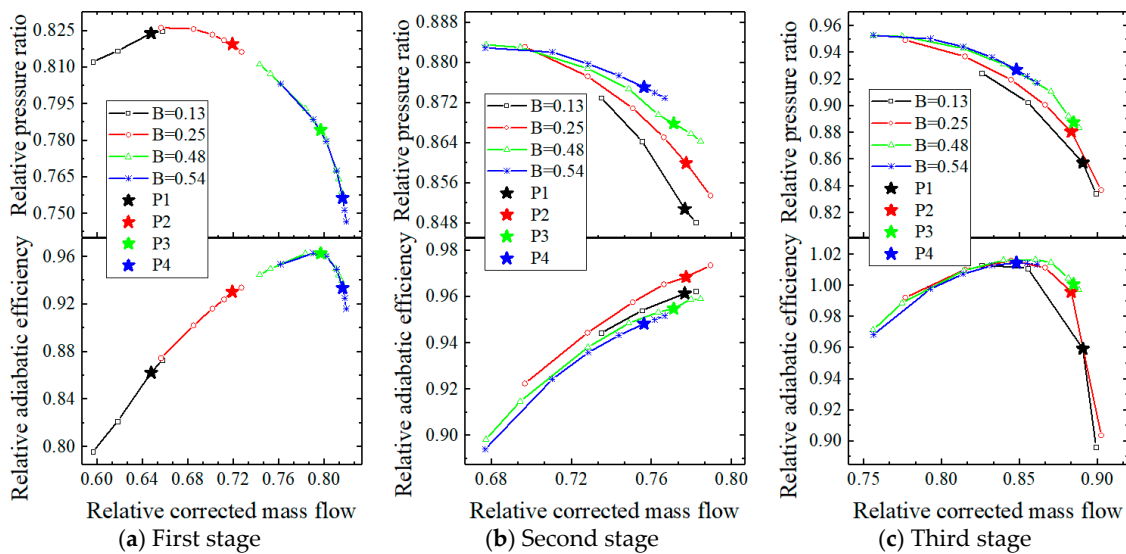


Figure 9. The characteristics for each stage of the “1 + 2” split fans at 80% RPM.

As the bypass ratio increases, the overall characteristic lines of the “1 + 2” split fans shift toward higher values with an accompanying increase in the total flow capacity. Simultaneously, there is an initial rise followed by a decline in peak efficiency as the bypass ratio increases. However, at 80% rpm, the “1 + 2” split fans have only the first stage as the bypass ratio increases and the flow capacity at the operating points increases away from the stall boundary and close to the choking state, as shown in Figure 9a (operating points P1 → P4). With the increase in the bypass ratio, there is a decrease in the flow capacity at the operating points of the second and third stages within the inner duct of the split fans, approaching closer to the stall boundary, as depicted in Figure 9b,c (operating points P1 → P4).

Comparing the characteristics of the two types of split fans in terms of their bypass ratios at 80% rpm, it is evident that as the bypass ratio increases, the peak efficiency of both split fans initially rises and subsequently declines. Simultaneously, the total flow capacity of these split fans exhibits an initial increase until a certain bypass ratio is reached, beyond

which there is no further change in the flow capacity. In this study, when the “2 + 1” split fans just reach the maximum flow capacity, the corresponding bypass ratio is 0.3, whereas when the “1 + 2” split fans just reach the maximum flow capacity, the associated bypass ratio is 0.48.

#### 4. Analysis of the Flow Capacity of the Different Split Fans

The operating points (Q1, Q2, Q3, and Q4 of “2 + 1” and P1, P2, P3, and P4 of “1 + 2”) selected in this study at 80% rpm essentially represent the flow capacity of the split fans under different bypass ratios. Figure 10 presents a comparative analysis of the flow capacity at different operating points of the split fans with varying bypass ratios. The results indicate that, with an increasing bypass ratio, the flow capacity of the split fans initially shows an increase for these fans until it reaches a critical bypass ratio, beyond which it remains constant. For small bypass ratios, the flow capacity of the “1 + 2” split fans is either greater than or equal to that of the “2 + 1” split fans. At high bypass ratios, the maximum flow capacity of the “1 + 2” split fans remains greater than or equal to that of the “2 + 1” split fans. Furthermore, as the bypass ratio increases, there is a significantly faster increase in the flow capacity at the operating points of the “1 + 2” split fans compared to those of the “2 + 1” split fans.

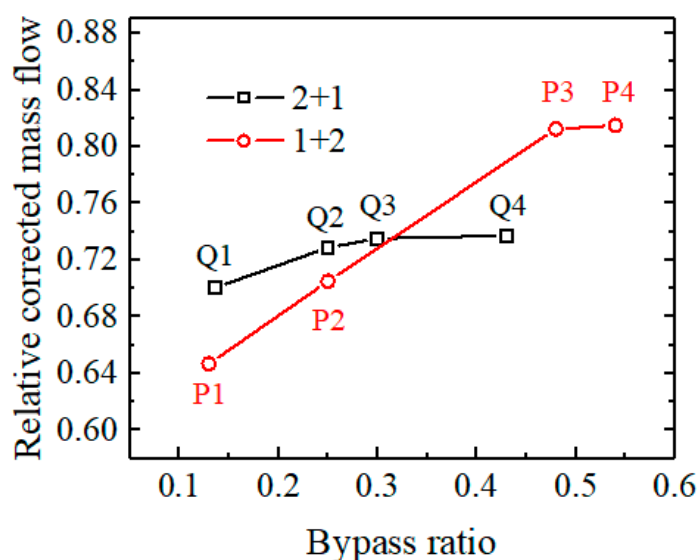
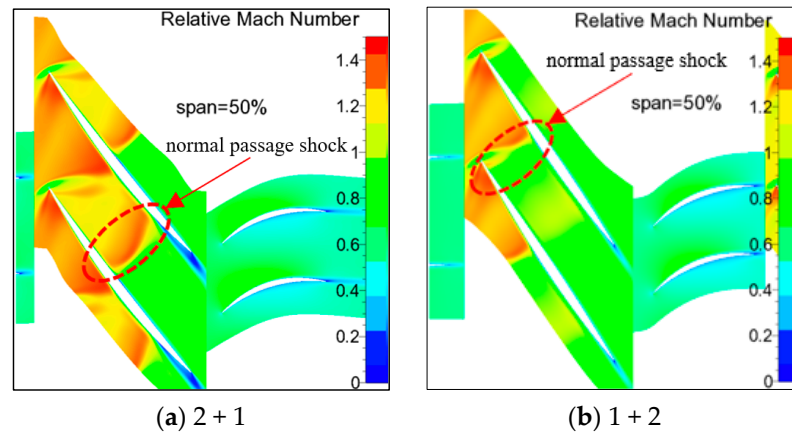


**Figure 10.** Variation in the flow capacity of the split fans at the operating points with bypass ratios.

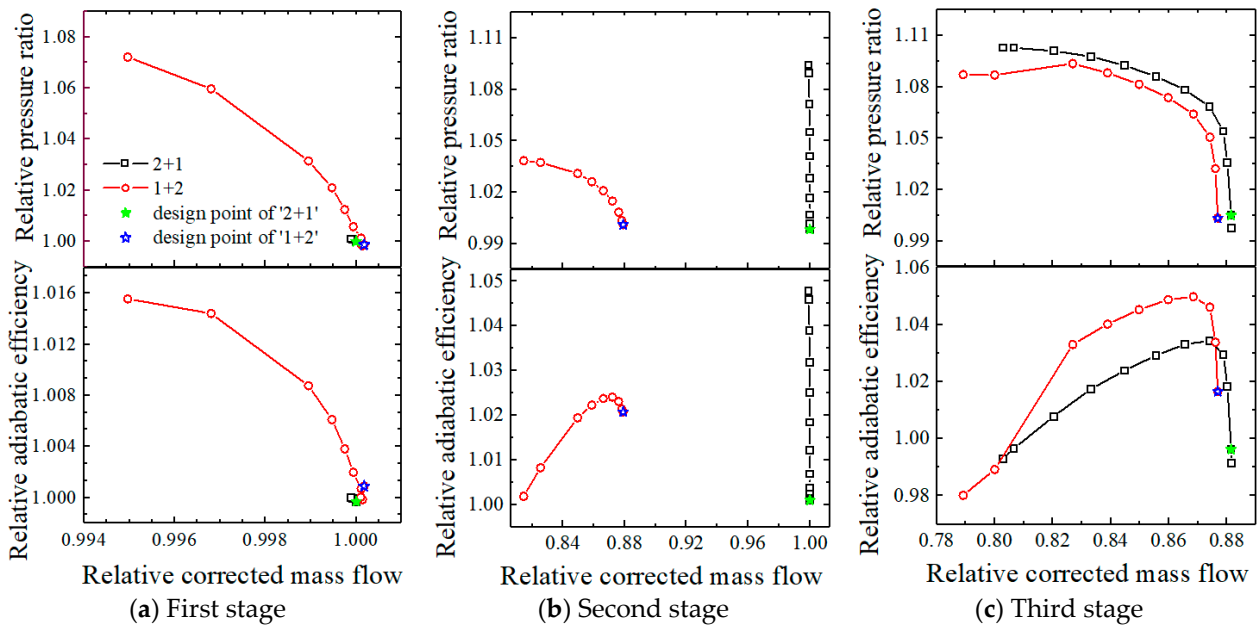
##### 4.1. Analysis of the Flow Capacity of the Split Fans with a Small Bypass Ratio

Figure 11 illustrates that the normal shock at the 50% blade height section of the second rotor’s design point in the “1 + 2” split fans approaches the inlet of the blade passage at 100% rpm. When combined with Figure 12b, it is evident that the design point of the second stage in the “1 + 2” split fans is proximate to its peak efficiency, exhibiting a weak choking condition and limited margin reserve for the rotor pressure ratio. In contrast, for the second rotor’s design point at the 50% blade height section of the “2 + 1” split fans, it features a double wave structure consisting of an inlet oblique shock followed by a normal passage shock, with this normal passage shock being further away from the inlet of the blade passage. In conjunction with Figure 12b, it can be observed that the design point of the second stage of the “2 + 1” split fans is the deep choking point on the characteristic line, resulting in a higher margin reserve for the rotor pressure ratio. This implies that the maximum total pressure achievable by the second stage of the “2 + 1” split fans is higher.





**Figure 11.** Mach contours of the 50% span at the second stage’s design point of the split fans at 100% rpm.



**Figure 12.** The characteristics for each stage of the split fans at 100% RPM.

When the corrected speed decreases and the split fans are in a state of having a small bypass ratio, the flow coefficient of both the first and second stage decreases, leading to their operating points approaching the stall boundary. Consequently, at this point, both pressure ratios for the first and second stages of the split fans are close to their respective maximum total pressure ratios. Therefore, as depicted in Figure 13b, due to its higher maximum total pressure rise, the second stage of the “2 + 1” split fans can achieve a higher matching pressure ratio. Additionally, since both configurations employ identical designs for their first stages, their matching pressure ratios are also similar (as shown in Figure 13a). However, this results in a higher inlet total pressure for the third stage of the “2 + 1” split fans (as shown in Figure 13c). Moreover, considering that both configurations have equal corrected mass flow rates at their respective operating points of the third stage, this implies that the “2 + 1” split fans’ third stage possesses a larger physical flow capacity. Therefore, the “2 + 1” split fans can achieve a higher flow capacity than the “1 + 2” split fans with a small bypass ratio at 80% rpm.

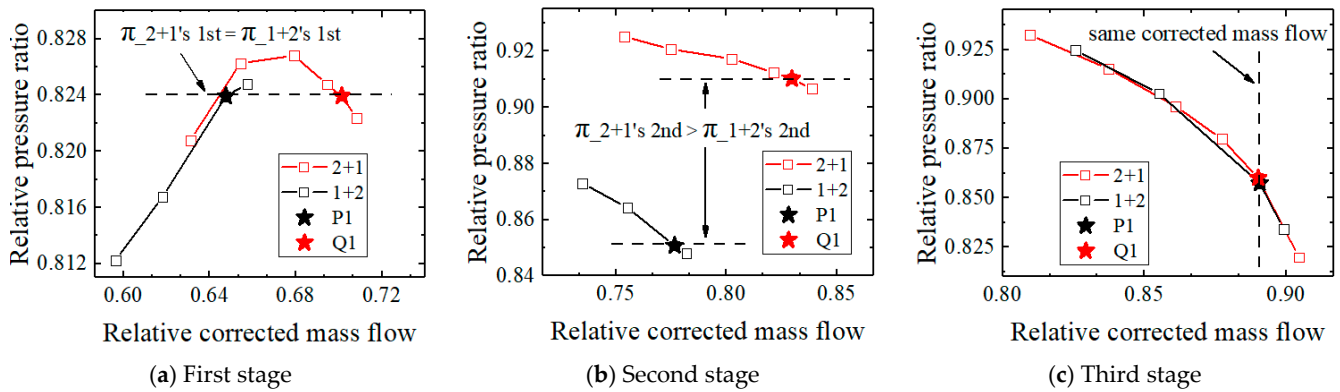


Figure 13. The characteristics of each stage of the split fans with a small bypass ratio at 80% speed.

Thus, while ensuring the efficiency at the design point of 100% rpm, it is necessary to maximize the pressure ratio margin of the second stage of the split fans in order to enhance its flow capacity at the middle speed when operating with a small bypass ratio.

4.2. Analysis of the Maximum Flow Capacity of the Split Fans

As illustrated in Figure 14a,b, shock waves can be observed only near the leading edge of the suction surface in the flow field of the first-stage rotor of the “1 + 2” split fans for small bypass ratios (operating points P1 and P2). With an increase in the bypass ratio, the shock wave gradually shifts rearward along the first-stage fan rotor. At a maximum flow capacity with high bypass ratios (operating points P3 and P4), as depicted in Figure 14c,d, a normal passage shock wave emerges within the flow field of the first-stage rotor. Simultaneously, as shown in Figure 15a, no further change occurs in flow capacity at this operating point for the first-stage fan (operating points P3 → P4). Therefore, it can be inferred that at this juncture, essentially choked conditions prevail for the operation of the first-stage fan.

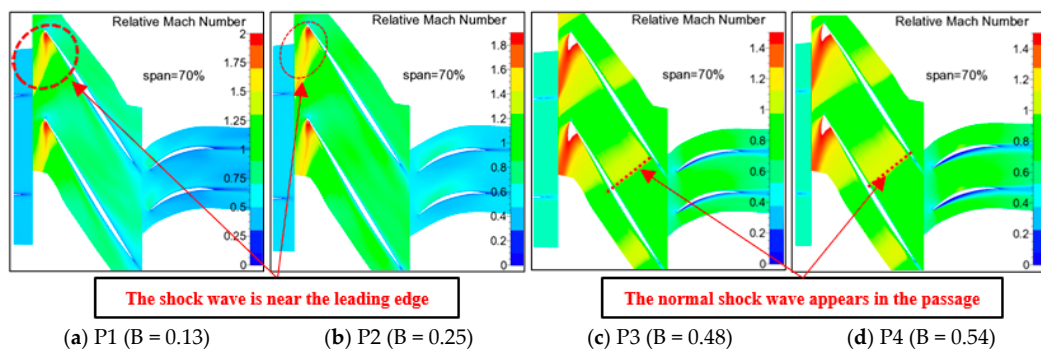


Figure 14. Mach number contours of the 70% section at operating points of the front fan in the “1 + 2” split fans with different bypass ratios. (Red dashed circles mark the position of the shock wave).

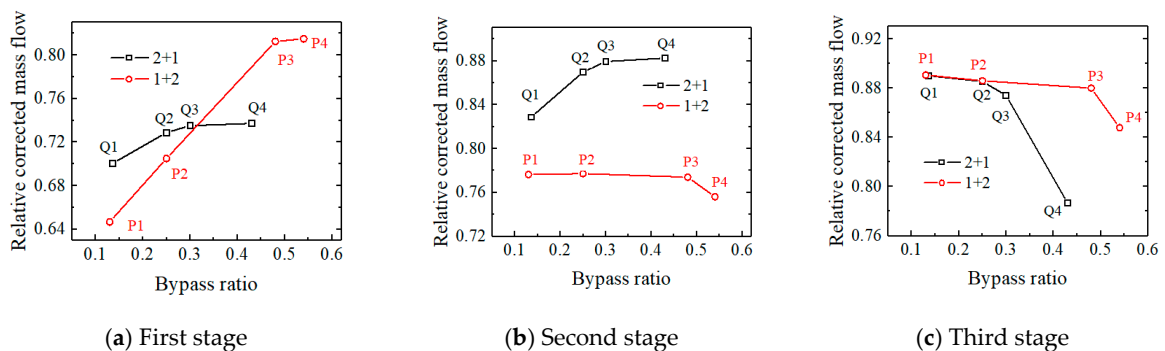
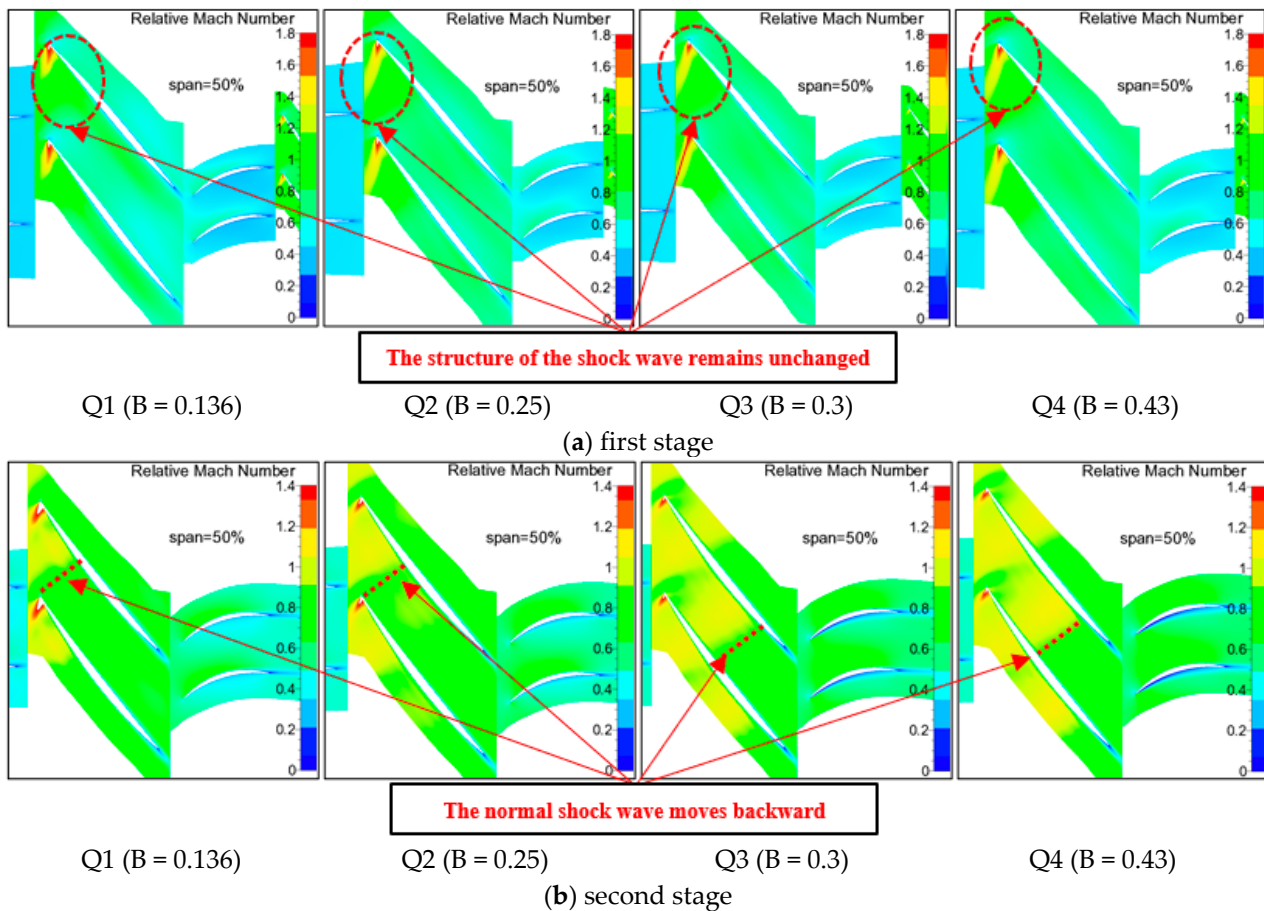


Figure 15. Variation in the relative flow at operating points with bypass ratios.

When the “2 + 1” split fans reach the maximum flow capacity (that is, when the bypass ratio is greater than 0.3, the operating points are Q3 and Q4), as shown in Figure 16b, a normal shock wave occurs in the passage at the rotor of the second-stage fan. Simultaneously, as shown in Figure 15, the flow capacity at the operating point of the second-stage fan will no longer change (operating points Q3 → Q4), so the second stage is basically choked. However, at this time, as shown in Figure 16a, only a shock wave appears at the leading edge of the suction surface for the rotor at the operating point of the first-stage fan, remaining far from reaching a choking state. Obviously, only when the first stage is choked can the flow capacity of the split fans reach the maximum. Therefore, the maximum flow capacity of the “1 + 2” split fans is greater than that of the “2 + 1” split fans.



**Figure 16.** Mach number contours of the 50% section at operating points of the front fan in the “2 + 1” split fans with different bypass ratios.

#### 4.3. Analysis of the Rate of Change in the Flow Capacity for the Split Fans

As shown in Figures 17 and 18, when the bypass ratio of the “2 + 1” split fans is less than 0.3, or the bypass ratio of the “1 + 2” split fans is less than 0.48, the flow field at the operating points of the third-stage fan is represented by the mid-blade section, the inlet shock wave of the rotor passage is sealed, and the rotor is basically choked. At this time, the corrected mass flow of the third-stage fan does not change with the bypass ratio, as shown in Figure 15c (operating points Q1 to Q3 and P1 to P3). When the bypass ratio of the “2 + 1” split fans reaches 0.43 or the bypass ratio of the “1 + 2” split fans reaches 0.54, the increase in the mass flow of the bypass makes the operating points of the third stage fan out of the choking state, the inlet shock wave is pushed out, and the corrected mass flow of the third stage fan is significantly reduced, as shown in Figure 15c (operating points Q4 and P3).

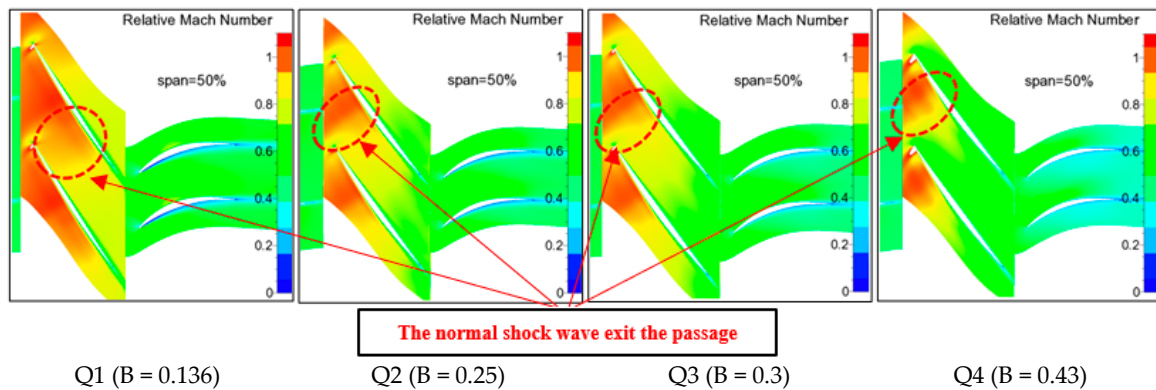


**Figure 17.** Mach number contours of the 50% section at operating points of the third stage fan in the “2 + 1” split fans with different bypass ratios.

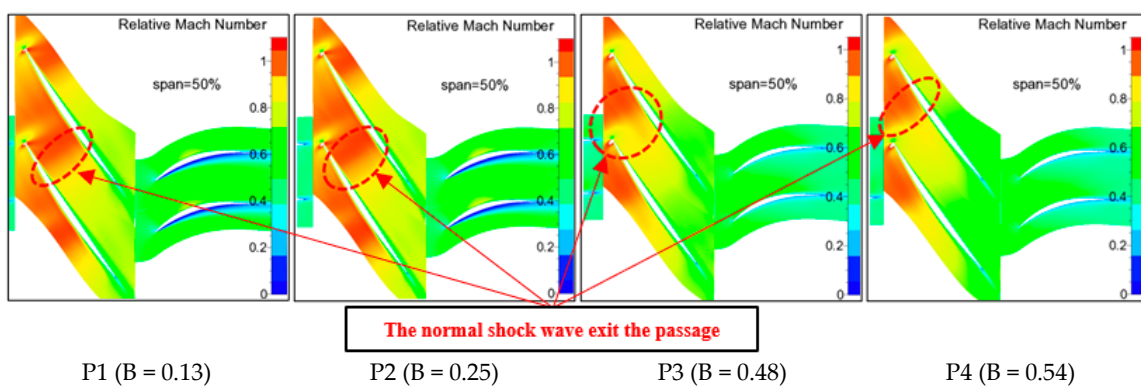


**Figure 18.** Mach number contours of the 50% section at operating points of the third stage fan in the “1 + 2” split fans with different bypass ratios.

The above analysis indicates that when the bypass ratio of the “2 + 1” split fans is less than 0.3 (i.e., Q1 → Q3) or the bypass ratio of the “1 + 2” split fans is less than 0.48 (i.e., P1 → P3), the operating point of the third stage fan is choked. The split fans reduce the back pressure of the bypass and increase the matching mass flow of the front fan, resulting in a decrease in the matching pressure ratio of the front fan, which leads to reduced total parameters at the rear fan inlet, decreased physical mass flow, and an increased bypass ratio for the split fans.

Therefore, as shown in Figure 19, with the increase in the bypass ratio, the pressure ratio of the first stage and the second stage in the “2 + 1” split fans decreases. However, due to the blockage of the third stage fan, only the pressure ratio of the first stage in the “1 + 2” split fans decreases, and the pressure ratio of the second stage fan is almost unchanged. In short, the decrease in the total inlet pressure of the third stage fan in the “2 + 1” split fans is significantly greater than that in the “1 + 2” split fans.

Thus, as shown in Figure 20, in the “2 + 1” split fans, the physical mass flow of the third-stage fan (i.e., the physical mass flow of the inner duct) decreases more significantly with an increase in the bypass ratio compared to the “1 + 2” split fans, when the corrected mass flow remains constant (the y-axis represents the ratio of the physical mass flow at the current operating point to the physical mass flow at the design point at 100% rpm). According to the definition of the bypass ratio, the mass flow at the inlet of the split fans is  $(1 + B)$  times the mass flow of the inner duct. When the increase in the bypass ratio is the same, the physical mass flow of the inner duct of the “2 + 1” split fans decreases more. Consequently, the increase in the mass flow at the inlet of the “2 + 1” split fans is smaller (as shown in Figure 10).

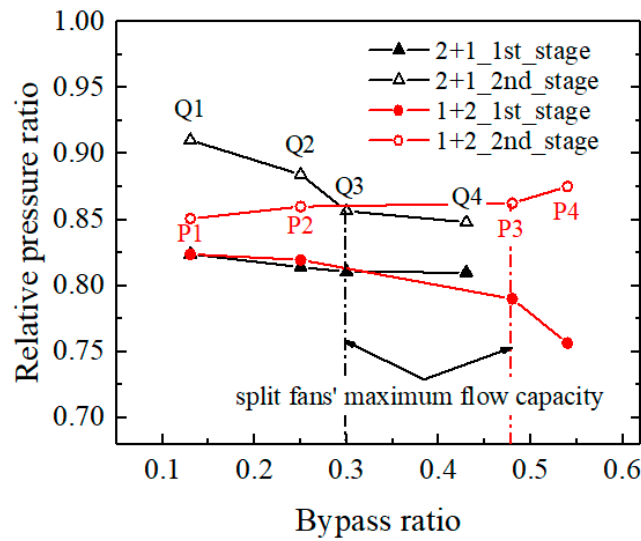


**Figure 19.** Variation in the relative pressure ratio of the first two stages of the split fans with bypass ratios.

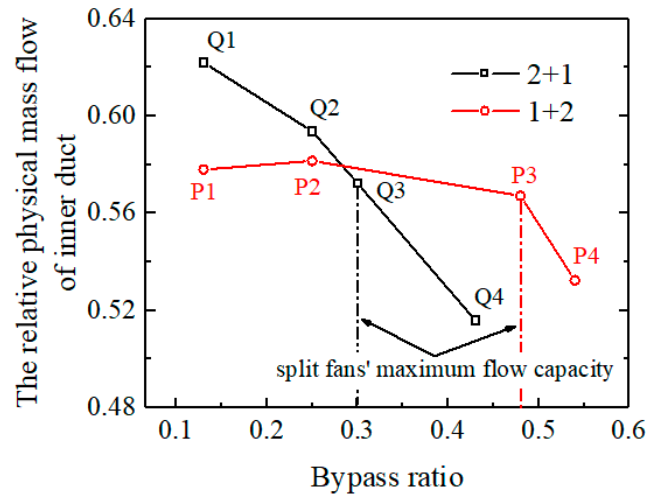


**Figure 20.** Variation in the relative physical mass flow of the inner duct with bypass ratios.

### 5. Analysis of the Efficient–Stable Operating Regions of the Different Split Fans

The efficiency and stall margin of the split fans’ operating points with respect to their bypass ratio are summarized in this section, providing a comprehensive region of the efficient and stable operating conditions for different split fans. Subsequently, the optimal bypass ratio of the different split fans was analyzed according to the variation in the flow capacity of the split fans. Finally, an analysis was conducted to elucidate the physical mechanism underlying the existence of an optimal bypass ratio for the split fans.

#### 5.1. Variation in the Efficiency of the Split Fans with Bypass Ratios

As depicted in Figure 21, the adiabatic efficiency gradually increases with an increasing bypass ratio at operating points for both the “2 + 1” split fans (with a bypass ratio of 0.3, operating point Q3) and the “1 + 2” split fans (with a bypass ratio of 0.48, operating point P3), until it reaches its maximum flow capacity. At this point, both types of split fans achieve their peak efficiency. Subsequently, as the bypass ratio continues to increase, the efficiency of both types starts to decline. Ultimately, the determination of the relative efficient region for the split fans shown in Figure 21 is based on a peak efficiency decrease within a limit of 0.2%.

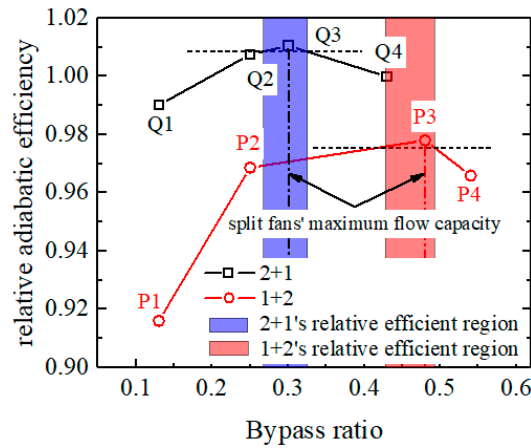


**Figure 21.** Variation in the efficiency of the different split fans with bypass ratios.

5.2. Variation in the Stall Margin of the Split Fans with Bypass Ratios

As shown in Figure 22, similar to the bypass ratio corresponding to the optimal efficiency, with an increase in the bypass ratio, when the split fans approach the maximum flow capacity, the stall margin of the operating points of the split fans reaches a maximum value. Therefore, with an increase in the bypass ratio, the stall margin of both the “2 + 1” and “1 + 2” split fans increases first and then decreases. The stable operating range of the split fans in Figure 22 was ultimately determined, ensuring a minimum stall margin of 20%.

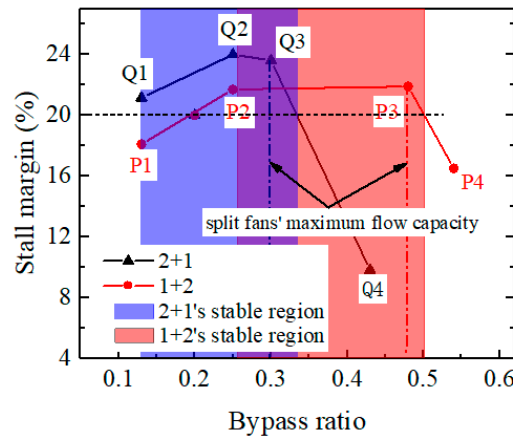


**Figure 22.** Variation in the stall margin with bypass ratios at the operating points of the different split fans.

5.3. The Optimal Bypass Ratio of the Different Split Fans

With the change in the bypass ratio, the operating point performance of the split fans has a relatively efficient region, as shown in Figure 21, and a stable operating region, as shown in Figure 22. Combining the two regions, the efficient–stable operating region of the split fans that simultaneously meets the efficiency and margin limits as shown in Figure 23 can be obtained. It is found from the figure that the “2 + 1” split fans’ operating point Q3 and the “1 + 2” split fans’ operating point P3, which have just reached their respective maximum flow capacity, are within the efficient–stable operating region. Therefore, when the split fans just reach their maximum flow capacity, the bypass ratio (operating point Q3 of the “2 + 1” split fans and operating point P3 of the “1 + 2” split fans) is the optimal bypass ratio. At this time, the split fans can not only reach their maximum flow capacity, but also achieve a stable and efficient operation.

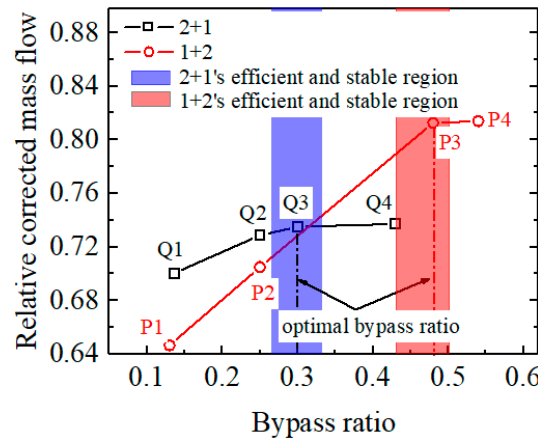


Figure 23. Stable and efficient operating regions of the different split fans.

5.4. Mechanism Analysis of the Optimal Bypass Ratio of the Split Fans

As the bypass ratio increases, when the split fans reach their maximum flow capacity (operating point Q3 of the “2 + 1” split fans and operating point P3 of the “1 + 2” split fans), nearly all shock wave structures in the rotor approach optimality, except for the first rotor of the “2 + 1” split fans, which is influenced by the choking state of the second stage, as shown by the Mach number contours of a typical section at the rotor’s operating point. Additionally, as depicted in Figure 24, taking the example of the “2 + 1” split fans to elucidate the mechanism, almost all stators operate near their optimal incidence at the operating points. Consequently, both the operating points of the front and rear fans are matched within their respective high-efficiency ranges. Therefore, both split fans achieve maximum efficiency. However, with a further increase in their bypass ratio, both the rotors and stators gradually deviate from their respective optimal flow states, leading to a decline in efficiency for both split fans.

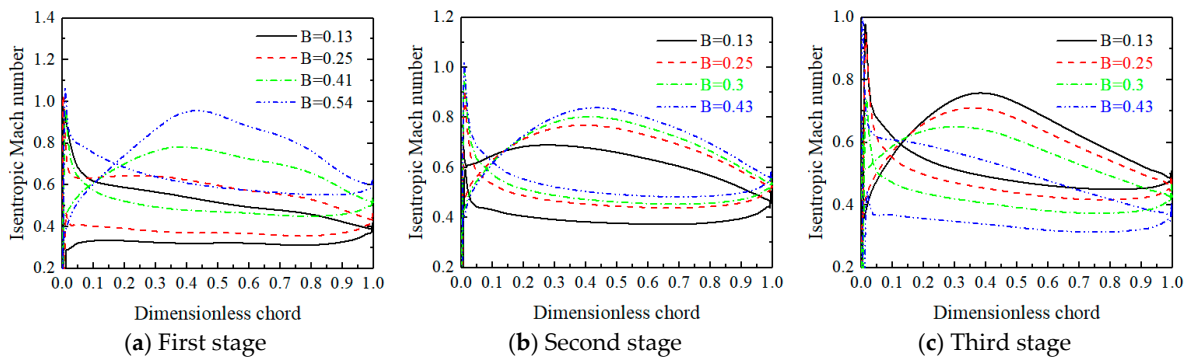


Figure 24. Isentropic Mach number distributions on the blade surface of each stator of the “2 + 1” split fans at the 50% blade height.

Similar to the optimal efficiency, with an increase in the bypass ratios, for either the “2 + 1” or “1 + 2” split fans as shown in Figures 7 and 9, the operating points of the front fan gradually changes from a near-stall state to a choking state, resulting in an increase in the stall margin of the split fans as that of the front fan, which experiences stalling first, increases. Meanwhile, the operating points of the rear fan gradually change from choked to near-stall, and the stall margin of the rear fan gradually decreases. Only with the matching condition of the front and rear fans being optimal, i.e., when the split fans approach the maximum flow capacity, does the stall margin of the split fans nearly approach the maximum. Subsequently, as the bypass ratio continues to increase, the stall margin of the rear fan decreases significantly. As a result, the rear fan experiences stalling first, leading to a decline in the stall margin of the split fans.

In conclusion, as shown in Figure 25, with the bypass ratio increasing, the flow capacity of the split fans initially shows an increase for these fans until it reaches a critical bypass ratio, beyond which it remains constant. Moreover, the efficiency and stall margin of the split fans are also close to the maximum at the critical bypass ratio, so the critical bypass ratio is the optimal bypass ratio of the split fans.

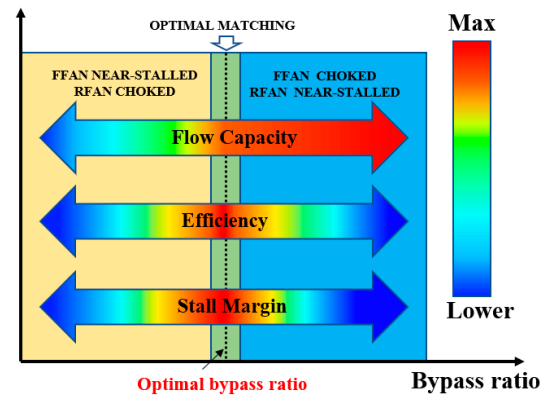


Figure 25. Variation in the aerodynamic performance of the split fans with bypass ratios.

## 6. Conclusions

The flow capacity and efficient–stable working region of two types of variable cycle split fans, namely “1 + 2” and “2 + 1” operating at 80% rpm, were studied in this paper. Additionally, the underlying physical mechanism behind their performance was analyzed. Our conclusions are summarized as the following:

1. The peak efficiency of both types of split fans exhibits an increasing trend followed by a subsequent decrease as the bypass ratio increases at 80% rpm. Moreover, the flow capacity initially shows an increase for these fans until it reaches a critical bypass ratio, beyond which it remains constant. Specifically, the “2 + 1” split fans achieve a maximum flow capacity at a bypass ratio of 0.3, while for the “1 + 2” split fans, it occurs at 0.48.
2. Under the condition of a small bypass ratio at 80% rpm, the first two stages of the two split fans are close to stall, while the third stage fan is choked, and the total inlet parameters of the third stage of the “2 + 1” split fans with a higher matching pressure ratio of the second stage fan are higher. Consequently, the “2 + 1” split fans can achieve a greater flow capacity. Under the condition of the high bypass ratio at 80% rpm, the first stage of the “1 + 2” front fan experiences flow choking, while the second stage of the “2 + 1” front fan also undergoes flow choking, but the first stage remains close to stall. Obviously, only when the first stage reaches a choking state can the split fans achieve a greater maximum flow capacity. Therefore, the maximum flow capacity of the “1 + 2” split fans is greater than or equal to that of the “2 + 1” split fans.
3. As the bypass ratio increases, the flow capacity of the front fan of the split fans also increases, causing its operating points to shift toward the deep choking state at the lower right of the characteristic line. Consequently, there is a decrease in the matching pressure ratio for the front fan and subsequently, a reduction in the total inlet pressure for the rear fan. The reduction in the matching pressure ratio is more pronounced for the front fan of the “2 + 1” split fans compared to that of “1 + 2” split fans, resulting in a faster decline in the physical mass flow within the inner duct and a significantly lower rate of increase for the corresponding flow capacity of the split fans.
4. When the flow capacity of the split fans reaches its maximum, the matching state of the front and rear fans achieves optimal performance—with rotors and stators at all stages being nearly perfectly matched near the best incidences. Consequently, both the efficiency and stall margin approach their peak values at this point. Simultaneously, the corresponding bypass ratio represents the optimal bypass ratio for the split fans.



**Author Contributions:** Conceptualization, G.A.; methodology, G.A. and R.Z.; validation, R.Z. and G.W.; formal analysis, G.A. and R.Z.; resources, X.Y. and B.L.; data curation, G.W.; writing—original draft preparation, G.A. and R.Z.; writing—review and editing, G.A. and R.Z.; supervision, X.Y. and B.L.; project administration, X.Y.; funding acquisition, X.Y. and B.L. All authors have read and agreed to the published version of the manuscript.

**Funding:** This work was supported by the Aero-Engines and Gas Turbines Basic Science Center Project, Grant No. P2022-A-II-001-001, National Defense Science and Technology Key Laboratory Fund Project, Grant No. 2023-JCJQ-LB-063-0204, and Fundamental Research Funds for the Central Universities, Grant No. 501QYZX2023146001.

**Data Availability Statement:** Data are contained within the article.

**Conflicts of Interest:** The authors declare no conflicts of interest.

## Nomenclature

$\pi$	Total pressure ratio
$\theta$	Total temperature ratio
$\eta$	Adiabatic efficiency
$k$	Turbulence kinetic energy
$B$	Bypass ratio
$\dot{m}_{bypass}$	Mass flow rates of the bypass
$\dot{m}_{inner}$	Mass flow rates of the inner duct
$rpm$	Revolutions per minute
$IGV_i$	Inlet guide vane
$R_i$	Rotor
$S_i$	Stator
"1 + 2" or "2 + 1"	Configuration of split fans
FFAN	Front fan
REAN	Rear fan
$P1\sim P4\backslash Q1\sim Q4$	Operating points
NUMECA	3D CFD simulation software package

## References

1. Simmons, R.J. *Design and Control of a Variable Geometry Turbofan with an Independently Modulated Third Stream*; The Ohio State University: Columbus, OH, USA, 2009.
2. Li, B.; Chen, M.; Zhu, Z.L. Steady Performance Investigation on Various Modes of an Adaptive Cycle Aero-Engine. *J. Propuls. Technol.* **2013**, *34*, 1009–1015.
3. Chen, M.; Zhang, J.; Tang, H.L. Performance Analysis of a Three-Stream Adaptive Cycle Engine during Throttling. *Int. J. Aerosp. Eng.* **2018**, *2018*, 9237907. [[CrossRef](#)]
4. Han, J.; Wang, J.K.; Liang, C.Y.; Su, G.Y. Thrust performance optimization calculation and analysis of triple bypass variable cycle engine. *J. Aerosp. Power* **2018**, *33*, 338–344.
5. Allan, R.D. General Electric Company Variable Cycle Engine Technology Demonstrator Program. In Proceedings of the 15th Joint Propulsion Conference, Las Vegas, NV, USA, 18–20 June 1979.
6. Liu, Q.; Li, G.T.; Huang, H.C. Matching Simulation on Cycle Parameter of Triple Bypass Variable Cycle Engine. *Aeroengine* **2016**, *42*, 51–54.
7. Qi, H.B.; Huang, S.Z.; Wang, W.L.; Ding, C.X.; Chang, Y.B. Adaptive cycle engine performance design based on inlet/engine matching concept. *Gas Turbine Exp. Res.* **2016**, *29*, 5–10.
8. Giffin, R.G.; Ciokajlo, J.J.; Dunbar, L.W. Compressor Splitter for Use with a Forward Variable Area Bypass Injector. U.S. Patent 5680754, 28 October 1997.
9. Zheng, J.C.; Chen, M.; Tang, H.L. Matching mechanism analysis on an adaptive cycle engine. *Chin. J. Aeronaut.* **2017**, *30*, 706–718. [[CrossRef](#)]
10. Zheng, J.C.; Tang, H.L.; Chen, M.; Zhang, Y.J.; Zhuge, W.L. Operating Modes Performance Comparison Research in Typical Working Conditions on an Adaptive Cycle Engine. *J. Eng. Thermophys.* **2022**, *43*, 1743–1750.
11. Vdoviak, J.W.; Ebacker, J.A. VCE test bed engine for supersonic cruise research. *NASA Conf. Publ.* **1979**, *2108*, 347–356.
12. Yang, X.F.; Sun, T.L.; Meng, D.J.; Yin, H.B.; Wang, Y.M. Aerodynamic design method for core-driven fan stage considering multiple modes. *Acta Aeronaut. Astronaut. Sin.* **2024**, *45*, 128625.
13. Liu, B.J.; Jia, S.F.; Yu, X.J. Numerical Study of the Characteristics of a Variable Cycle Compressor. *J. Eng. Thermophys.* **2016**, *37*, 1850–1855.

14. Huang, L.; Zhang, J.; He, X.D.; Li, Q.H.; Chu, W.L.; Xiao, S.L. The matching performance research of core driven fan stage and compressor. *J. Aerosp. Power* **2023**. Available online: <https://kns.cnki.net/kcms2/detail/11.2297.V.20230717.1008.001.html> (accessed on 22 February 2024).
15. Ma, C.Y.; Hou, M.J.; Wang, H.; Gao, J. Matching Performance Prediction Between Core Driven Fan Stage and High Pressure Compressor. *Int. J. Turbo Jet-Engines* **2021**, *38*, 101–114. [[CrossRef](#)]
16. Shi, H. A Parametric Blade Design Method for High-Speed Axial Compressor. *Aerospace* **2021**, *8*, 271. [[CrossRef](#)]
17. Strazisar, A.J.; Wood, J.R.; Hathaway, M.D.; Suder, K.L. *Laser Anemometer Measurements in a Transonic Axial-Flow Fan Rotor*; Lewis Research Center, NASA: Cleveland, OH, USA, 1989; p. 214.

**Disclaimer/Publisher’s Note:** The statements, opinions and data contained in all publications are solely those of the individual author(s) and contributor(s) and not of MDPI and/or the editor(s). MDPI and/or the editor(s) disclaim responsibility for any injury to people or property resulting from any ideas, methods, instructions or products referred to in the content.